DOI: 10.1002/ejic.200800091

DFT and Experimental Studies of Perchlorate Ion Coordination in *cis*/*trans*-Copper(II) Complexes of Tetradentate Pyridyl Ligands

Thangarasu Pandiyan,*[a] Hernández J. Guadalupe,[b] Julian Cruz,[c] Sylvain Bernès,[d] Víctor M. Ugalde-Salvdivar,[a] and Ignacio González[e]

Keywords: Copper / Isomers / Density functional calculations / Redox chemistry

Spectral and structural studies of *N*,*N*′-dimethyl-*N*,*N*′-bis-(pyridin-2-ylmethyl)-1,2-diaminoethane (L^1), *N*,*N*′-dimethyl-*N*,*N*′-bis(pyridin-2-ylmethyl)-1,3-diaminopropane (L^2), and their copper(II) complexes were carried out by spectroscopic and DFT methods. The DFT results show that conventional and nonconventional H-bonds present in L^1 and L^2 influence the NMR chemical shifts at different pH values, which thus suggests that the protonation sites at the pyridyl and tertiary nitrogen atoms of the ligands change the chemical environment of the adjacent carbon atoms; this observation is consistent with ^{13}C NMR spectra recorded at different pH values. Furthermore, for their copper complexes, two possible geometrical isomers (*cis* and *trans*) are obtained; for example, *cis*-$[CuL^1]^{2+}$, where both NCH_3 groups are oriented in the same plane, is in equilibrium with its *trans* isomer and, as a result, a small energy difference (0.9 kcal mol^{-1}) appears. In contrast, *trans*-$[CuL^2]^{2+}$ does not equilibrate with the *cis* isomer, because there is a greater energy difference (ΔE = 3.9 kcal mol^{-1}) between the two isomers. Indeed, when $[CuL^1]^{2+}$ with two perchlorate ions was optimized, it was found that although only *cis*-$[CuL^1]^{2+}$ was able to accommodate a perchlorate ion in the axial position of the square pyramidal geometry by stabilizing the structure with two *cis* NCH_3 groups through H-bonds, the *trans* isomer was unable to retain the perchlorate ion in the coordination sphere, because the NCH_3 groups were in the *trans* position; this disfavors the presence of the perchlorate ion in the sphere, because of the absence of H-bonds. This is consistent with the X-ray structure, in which *cis*-$[CuL^1(ClO_4)]^+$ is resolved, whereas the *trans* isomer is not.

Introduction

Copper complexes are known to play important roles in the active sites of many copper proteins in vivo, as well as in homogeneous catalysis for organic chemical reactions;[1–13] they also act as functional catalysts and biological models for metalloproteins and participate in oxygen uptake.[14,15] Recent efforts in this area have involved the development of models that simulate the properties of copper proteins where copper(II) is present in an unusual geometry, and in which the models exhibit unique spectral properties in its biological function.[16,17] Copper complexes not only provide a better understanding of the biological systems, but also assist in the development of new homogeneous catalysts for selective oxidations.[18] This is the reason why there is extensive interest in studying copper complexes as potential models for metalloproteins.[18–25] Although a wide variety of supporting ligands are used to develop bioinorganic models in order to replicate the active-site structures and functions of copper proteins,[26] amine/pyridine ligands have been frequently used to prepare transition-metal complexes for diverse applications in biological studies;[27,28] recently, for example, the manganese(II) complex with the *N*-methyl-*N*,*N*′,*N*′-tris(pyridin-2-ylmethyl)-1,2-diaminoethane ligand has been used to describe the catalytic function of manganese superoxide dismutase[29] and the same ligand with iron has been employed to generate peroxo adducts with success.[30] Therefore, the tetradentate ligands containing amine and pyridyl groups are frequently employed to describe biological reactions. To study the geometrical behavior of tetradentate ligands with the copper(II) ion, *N*,*N*′-dimethyl-*N*,*N*′-bis(pyridin-2-ylmethyl)-1,2-diaminoethane (L^1) and *N*,*N*′-dimethyl-*N*,*N*′-bis(pyridin-2-ylmethyl)-1,3-diaminopropane (L^2) were synthesized and their chelating properties were analyzed at different pH values by ^{13}C NMR and GIAO-^{13}C NMR spectroscopy; furthermore, the

[a] Facultad de Química, Depto. de Quimica Inorgánica y Nuclear, Universidad Nacional Autónoma de México (UNAM), Ciudad Universitaria,
México D.F., 04510, México
E-mail: pandiyan@servidor.unam.mx
[b] Centro Tecnológico de la Escuela Nacional Profesionales, Universidad Nacional Autónoma de México (UNAM),
Aragon, Estado de México, México
[c] Centro de Investigaciones Químicas, Universidad Autónoma del Estado de Hidalgo, Unidad Universitaria,
Km 4.5 Carretera Pachuca-Tulancingo, C.P. 42184 Pachuca-Hidalgo, México
[d] DEP, Facultad de Ciencias Químicas, Universidad Autónoma de Nuevo León,
Monterrey, N. L., México
[e] Departamento de Quimica, Universidad Autónoma de México-Iztapalapa,
Apartado Postal 55-534, 09340 México D.F., México

geometrical analyses determined by DFT and X-ray analysis were used to interpret how the perchlorate ion is stabilized in the coordination sphere of the copper(II) complexes with the above ligands.

Results and Discussion

DFT Analysis of Ligands

In the present study, the structural and electronic parameters of the ligands were used to determine which of the conventional and nonconventional hydrogen bonds (H-bonds) influence the NMR chemical shift values. The conventional H-bond (Y–H–X); (Y or X = O, N, F etc.) is defined elsewhere,[31–35] and the most important geometrical criterion to confirm the existence of the H-bond is that the distance (H–X) should be smaller than the sum of the van der Waals radii of the H and X atoms. The nonconventional H-bonds (C–H–X) are usually weaker than the conventional ones (Y–H–X).

The ground-state geometries (Figures 1 and 2) of L^1 and L^2 were fully optimized in the neutral and protonated forms, and it was discovered that two possible conformers were present when the ligands were protonated. For example, the proton addition at the amine or pyridyl nitrogen atoms generates two structures, $L^1N8_{am}H^+$ (**1a**) and $L^1N1_{py}H^+$ (**1b**), of which **1a** is more stable than **1b** (energy difference is 6.46 kcal mol^{-1}). Furthermore, the bond lengths of the intramolecular nonconventional H-bonds N1···H–C10 (N1···H 2.50 Å) and N11···H–C14 (N11···H 2.56 Å) present in the L^1 structure are lower than that of the reported data[36,37] (sum of van der Waals radii: N···H 2.7 Å; N 1.5 Å, and H 1.1–1.2 Å). For its protonated structures ($L^1N8_{am}H$, **1a**), a conventional (N1···H–N8 1.89 Å) and a nonconventional (C9–H···N18 2.18 Å) H-bond are present, which implies that the protonation in $L^1N8_{am}H^+$ converts the nonconventional H-bond into a conventional H-bond. The same behavior is also noticed for **1b**, where one conventional H-bond (N1–H···N8 1.89 Å) and one nonconventional H-bond (C9–H···N1 2.31 Å) are present. In the case of ligand L^2 (Figure 2), no type of H-bond was found, but in its protonated structures only conventional H-bonds resulted (**2a**, N1···H–N8 1.95 Å; **2b**, N1–H···N8 1.95 Å). The energy of **2a** is lower by about 4.57 kcal mol^{-1} than that of **2b**, which thus suggests that **2a** is more stable than **2b**. Furthermore, the GS wave function of the ligand structures (AIM) clearly determines that bond critical points (BCPs) of CH–N contacts and ring critical point (RCP) of the structures (Figures 3 and 4) yield ρ and $\nabla^2\rho$ values, which thus confirms the presence of conventional, as well as nonconventional, H-bonds in the structures.

GIAO-^{13}C NMR and ^{13}C NMR Spectroscopic Studies

The determination of ^{13}C NMR chemical shift values was carried out by the GIAO method by using B3PW91/6-311++G** level theory for L^1 and L^2 and its protonated structures. The calculated chemical shifts were referenced to TMS (δ =187.24 ppm for carbon atoms and 31.86 ppm for protons in TMS). The results (Table 1) show that there is a strong influence of H-bond formation in the NMR signals. For example, in the L^1 structure, C2 (156.86), C3(125.77),

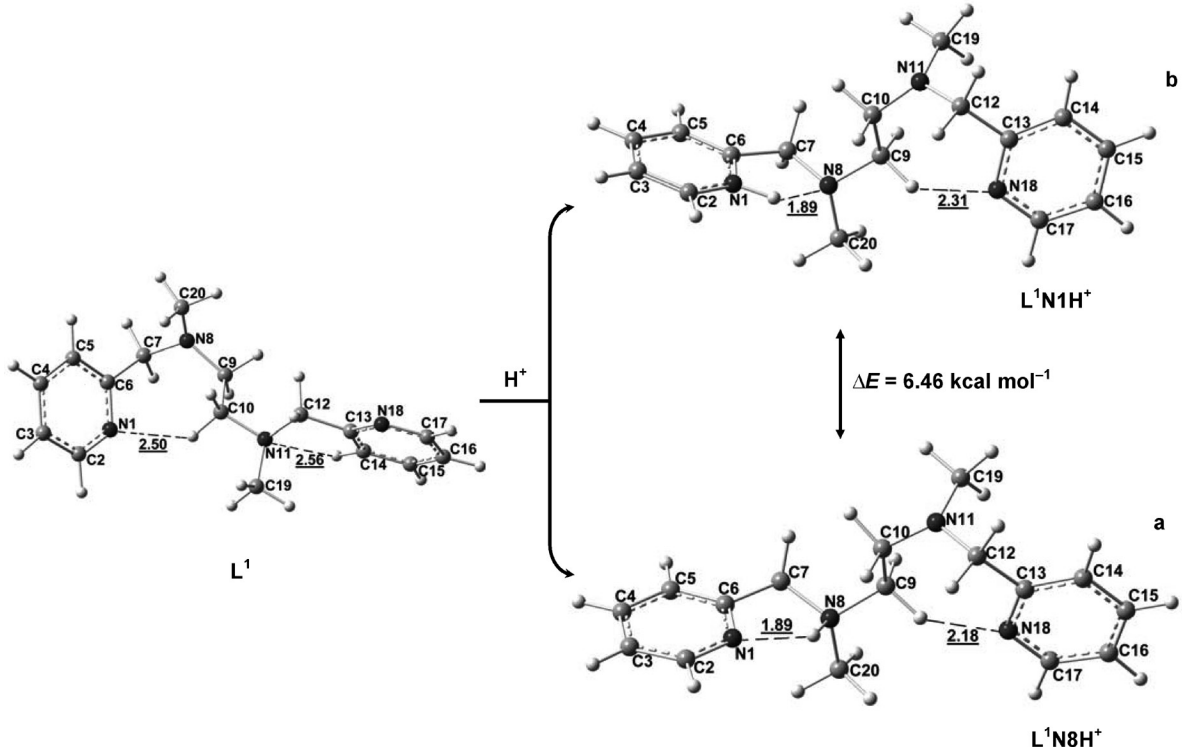

Figure 1. The optimized geometries of L^1 and its protonated structure.

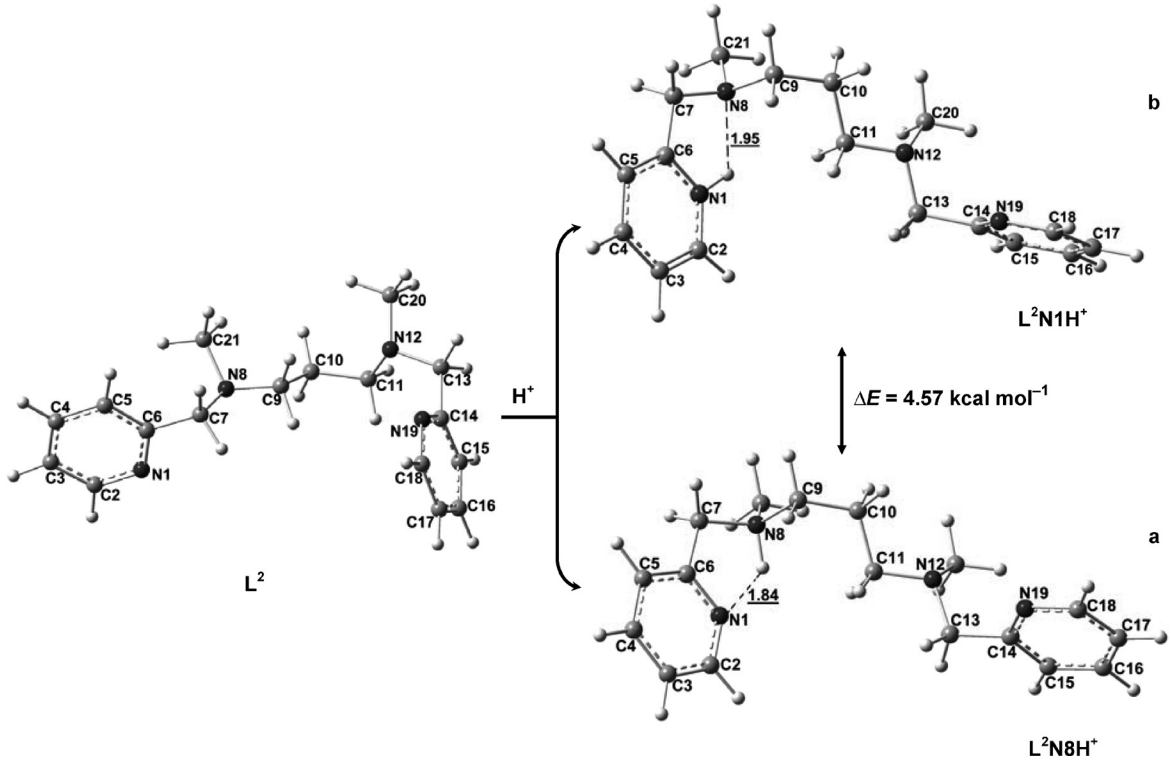

Figure 2. The optimized geometries of L^2 and its protonated structure.

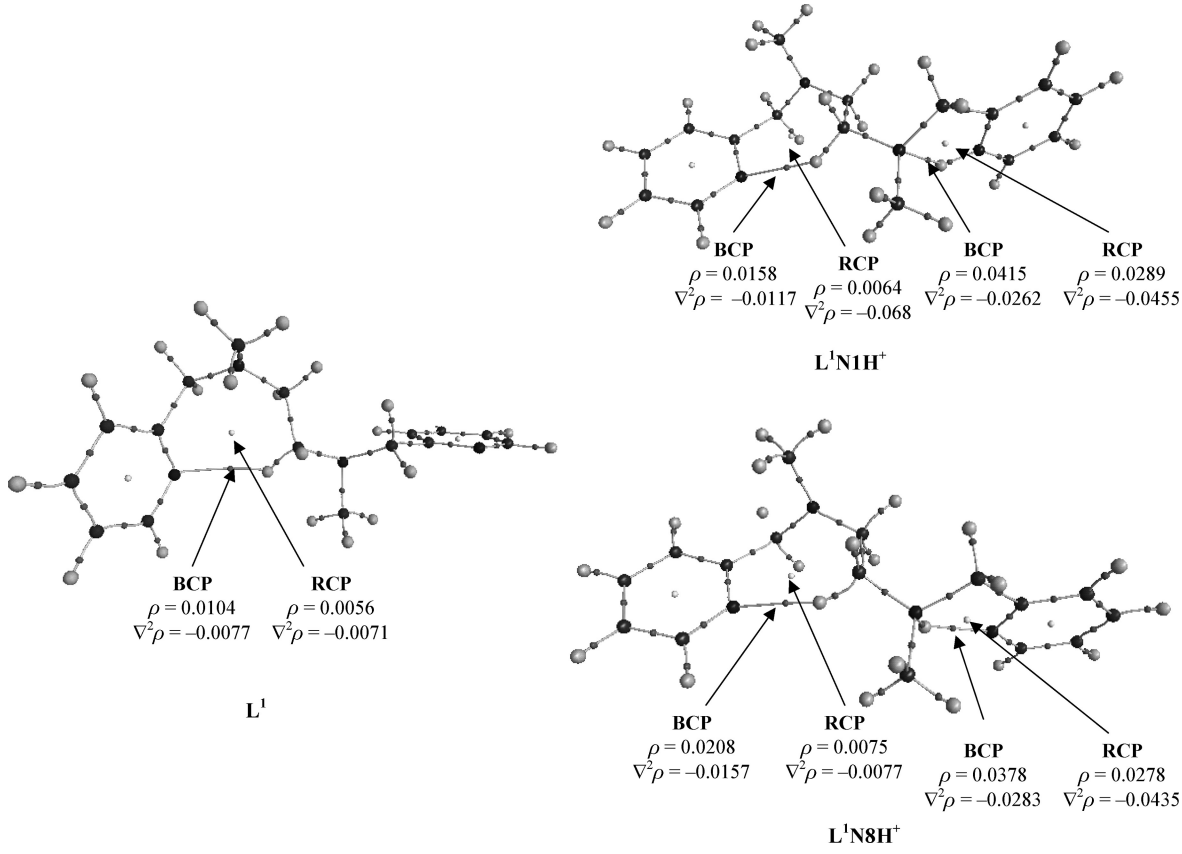

Figure 3. Bond critical points (BCPs) and ring critical point (RCP) of L^1.

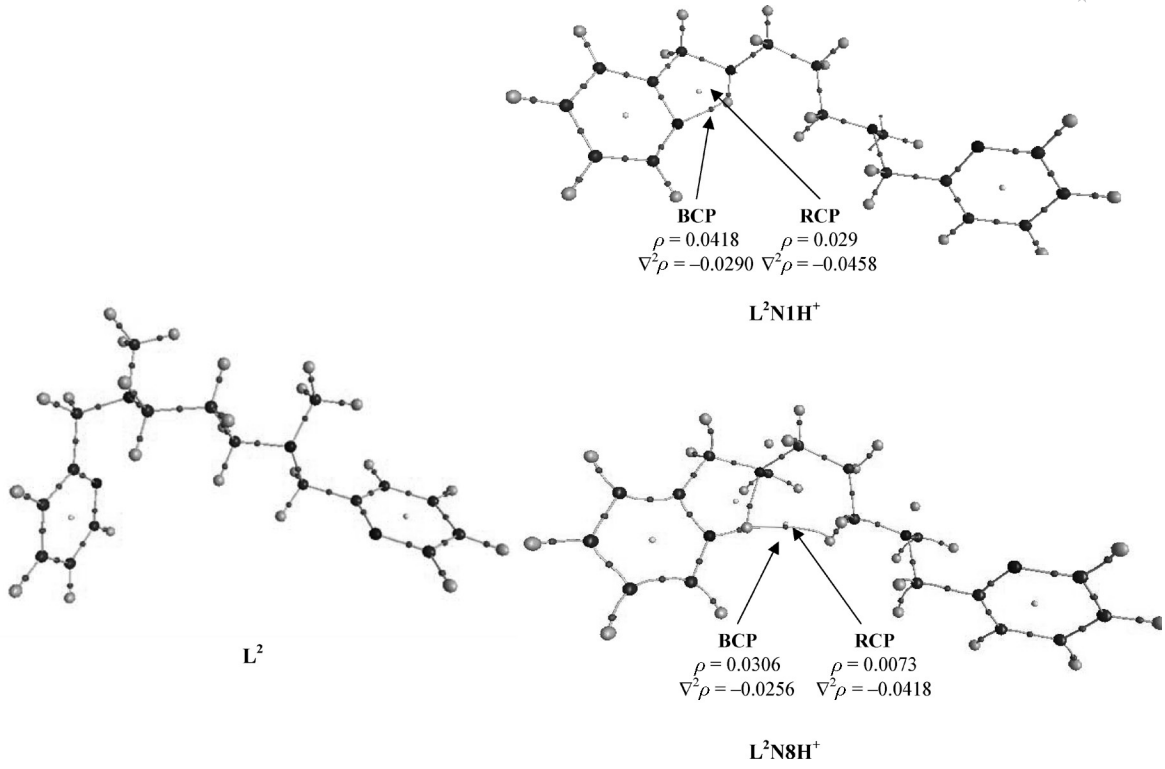

Figure 4. Bond critical points (BCPs) and ring critical point (RCP) of L^2.

Table 1. GIAO-^{13}C NMR parameters and charges of ligands.

Atom	^{13}C NMR chemical shift data			Charges		
	L^1	L^1N8H^+	$\Delta\delta$	L^1	L^1H^+	Δ
C2	156.86	155.44	1.42	–0.31	–0.17	0.14
C3	125.77	133.00	7.23	0.05	–0.15	0.20
C4	140.15	147.31	7.15	–0.72	–0.56	0.16
C5	128.04	127.83	0.21	0.44	0.18	0.26
C6	166.36	150.48	15.88	0.00	0.59	0.59
C7	67.09	61.20	5.90	–0.89	–1.54	0.65
C9	59.96	59.49	0.47	–0.56	–0.80	0.24
C10	54.01	57.21	3.20	–1.04	–0.68	0.36
C12	64.93	66.46	1.53	–1.04	–0.96	0.08
C13	169.66	165.81	3.85	–0.32	0.00	0.32
C14	125.75	130.38	4.63	0.77	0.45	0.33
C15	140.60	144.43	3.84	–0.95	–0.77	0.18
C16	125.32	129.03	3.71	0.09	–0.21	0.30
C17	155.37	154.52	0.85	–0.30	–0.07	0.24
C19	45.06	38.26	6.80	–0.42	–0.41	0.01
C20	39.34	45.69	6.35	–0.45	–0.43	0.01
Atom	L^2	L^2N8H^+	$\Delta\delta$	L^2	L^2H^+	Δ
C2	156.60	155.18	1.43	–0.33	–0.35	0.02
C3	125.80	132.94	7.14	0.09	0.09	0.01
C4	140.01	147.50	7.50	–0.74	–0.82	0.08
C5	129.27	127.82	1.45	0.65	0.45	0.21
C6	166.63	149.63	17.00	–0.27	0.14	0.41
C7	68.84	64.85	4.00	–0.91	–1.18	0.28
C9	54.95	61.70	6.75	–0.70	–0.43	0.27
C10	29.46	28.06	1.40	–0.33	–0.32	0.01
C11	61.14	58.06	3.08	–0.95	–1.12	0.17
C13	69.93	70.39	0.47	–0.95	–0.85	0.10
C14	166.99	162.30	4.69	–0.15	–0.21	0.05
C15	129.20	128.15	1.05	0.69	0.66	0.03
C16	139.66	141.63	1.98	–0.80	–0.80	0.00
C17	125.94	128.12	2.18	0.07	0.08	0.01
C18	156.71	157.59	0.89	–0.27	–0.27	0.00
C20	39.27	38.96	0.30	–0.46	–0.46	0.00
C21	43.13	40.37	2.75	–0.48	–0.51	0.03

C4 (140.15), and C6 (166.36) were predominantly affected when the protonation occurred at N8 (L^1N8_{am} H^+), which implies that after protonation (Figure 1), the nonconventional H-bonds N1–H···C10 (2.50 Å) and N11–H···C14 (2.56 Å) were changed into conventional (N1···H–N8 1.89 Å) and nonconventional (N18···H–C9 2.18 Å) H-bonds, which led to a change in the electronic structure; hence, the chemical shift of C2 and C6 decreased to 155.44 and 150.48 ppm and those of C3 and C4 increased to 133.00 and 147.31 ppm. Furthermore, it is interesting to note that because of the H-bonds, a five-membered ring that is planar to the pyridine ring was formed; this strongly shields C6 (localized), which thereby decreases its chemical shift from 166.36 to 150.48 ppm. Similarly, the nonconventional bond C9–H···N18 also affected the chemical shifts, for which the chemical shifts of C14, C15, and C16 increased, whereas that of C17 decreased; however, the effect of the nonconventional H-bond was obviously less than that of the conventional H-bond, as was observed in the chemicals shift and charge values. In contrast, owing to the limited formation of H-bonds because of the larger carbon chain in L^2 than that in L^1, only C6 was shielded by the presence of a conventional H-bond.

This theoretical interpretation coincides with the experimental ^{13}C NMR spectra of the ligands at different pH values. The spectra were recorded in D_2O at pH values between 3.0 and 8.0, and the influence of protonation/deprotonation sites of the ligands were analyzed by using chemical shift values of the carbon atoms adjacent to the pyridyl/tertiary nitrogen atoms. The results indicate that the methyl-

ene group attached to the tertiary and pyridyl nitrogen atoms manifest different behaviors in acidic and basic media. The results show that the ligands (L^1 and L^2) were protonated in acidic media, which reveals that none of the carbon atoms showed significant differences in chemical shift (δ) values except for those attached to the tertiary nitrogen atom, for which the δ value considerably decreased at low pH and increased at high pH. In contrast, for the pyridyl carbon atoms, δ values increased at low pH values and decreased at high pH, which suggests that both methylene groups attached to the tertiary and pyridyl nitrogen atoms behaved differently when the pH values were varied, that is, the chemical shift value gradually increased for methylene carbon atoms and slightly decreased for pyridyl carbon atoms (Figure 5). This explains how at low pH values the carbon atoms are more shielded (localized) by protonation of the tertiary nitrogen atom and, reversibly, are deshielded by the deprotonation process in basic media. When the protonation occurred at the tertiary nitrogen atom, the methylene group became more localized; thus, the δ value slightly increased. In the case of the pyridyl group, an opposite situation was observed due to the presence of electron deficiency in the pyridyl ring. However, the addition of a base to the ligands induced a very small shift, whereas the addition of acid to the ligands had little effect on the chemical shift value, which confirms the fact that the ligands behave as good Lewis bases rather than as acids and are suitable for the coordination of metal ions. Furthermore, the analysis of charges and HOMO orbitals indicates that the excess electron density over the nitrogen atoms is responsible for the bond formation with a metal ion. In addition, the hardness of the ligands was calculated to show the coordinating efficiency of the ligands with the Cu^{II} ion. The hardness of the molecules was determined by LUMO–HOMO/2. The results are 2.17 eV for L^1 and 2.29 eV for L^2, which indicates that L^2 coordinates more strongly with copper(II) (8.3 eV)[38,39] than L^1.

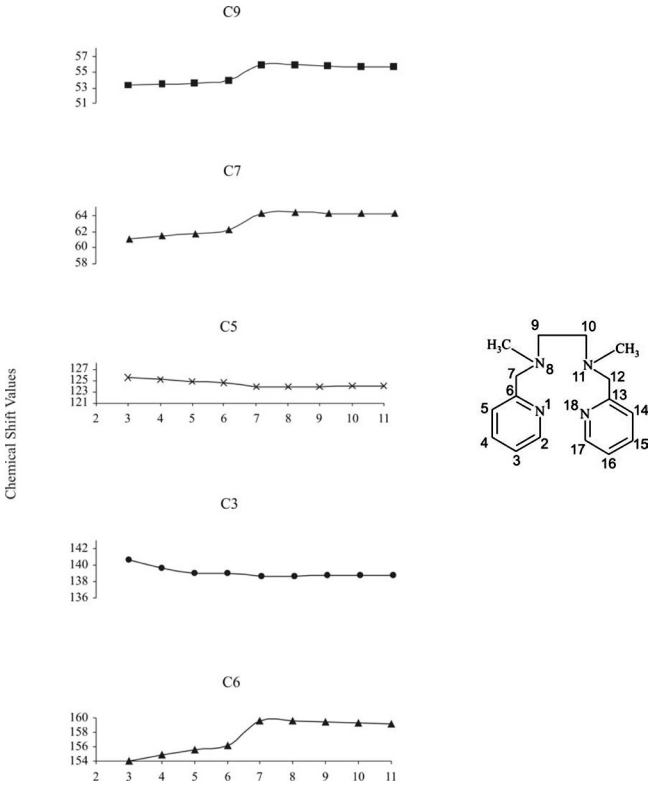

Figure 5. ^{13}C NMR spectra of L^1 at different pH values.

Optimized Geometrical Features of $[CuL^1]^{2+}$ and $[CuL^2]^{2+}$

The geometrical optimization of L^1 and L^2 with Cu^{II} was carried out by U-B3PW91 with base set 6-311++G** for C, N, and H atoms, and LANL2DZ pseudopotential for Cu^{2+} (Figures 6 and 7), and it showed that with copper(II), four bonds were formed by two amine and two pyridyl nitrogen atoms and that the pyridyl nitrogen atom formed a stronger bond (2.00–2.04 Å) than the amine nitrogen atom (2.05–2.08 Å), as the former was present in sp^2 hybridization, which involves backbonding with copper(II). In $[CuL^1]^{2+}$, the Cu^{II} ion showed a distorted plane, because of the ring strain caused by 5–5–5 chelate rings around the copper ion; in contrast, in $[CuL^2]^{2+}$, the Cu^{II} ion appeared in a perfect plane due to 5–6–5 chelate rings, and the central six-membered ring was found in a chair conformation, which results in a shorter bond length (Cu–Npy 2.00 Å).

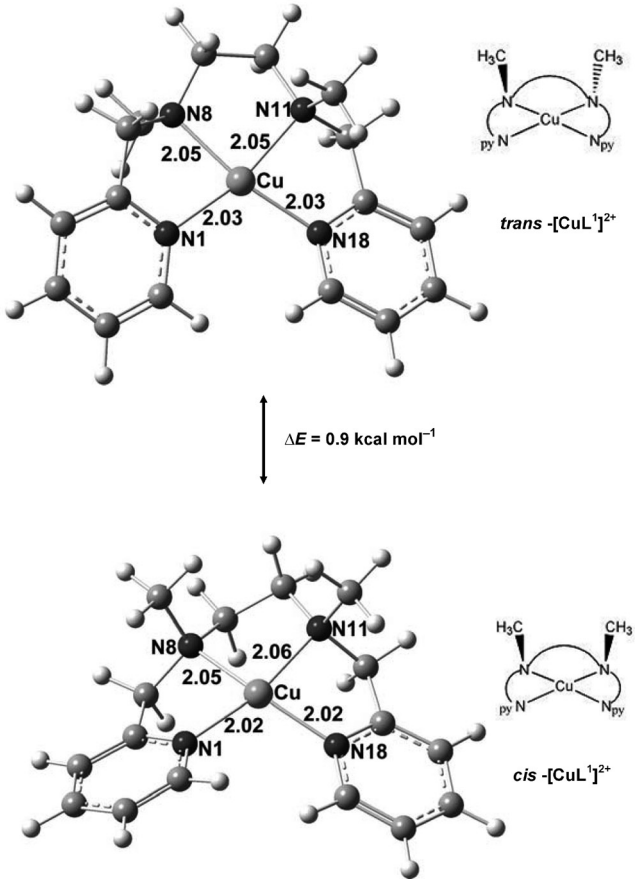

Figure 6. Optimized geometry of Cu^{II} with L^1 and its presence in the *cis and trans* isomers.

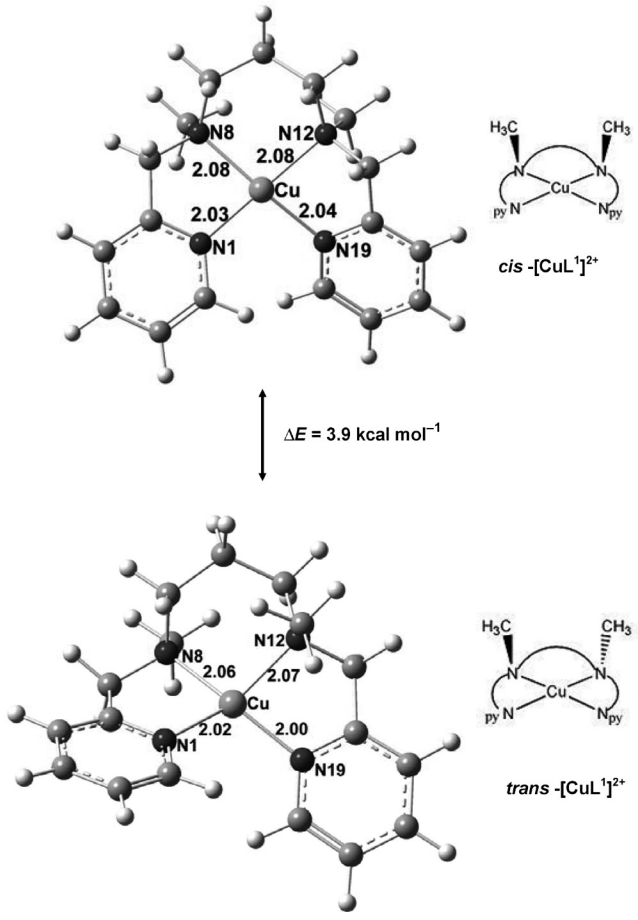

Figure 7. Optimized geometry of Cu^{II} with L^2 and its presence in the *cis and trans* isomers.

Furthermore, there were two possible geometrical isomers (*cis* and *trans*) for the complexes, that is, both NCH_3 groups were on the same side of the plane for the *cis* isomer, and one NCH_3 group was *trans* to the other NCH_3 group in the plane for the *trans* isomer (Figure 6). For $[CuL^1]^{2+}$, a small energy difference (0.9 kcal mol^{-1}) between the *cis* and *trans* configurations resulted, which suggests that both the *trans* and *cis* isomers were in equilibrium; however, a greater energy difference (ΔE = 3.9 kcal mol^{-1}) between the two isomers resulted for $[CuL^2]^{2+}$ (Figure 7), which shows that the *trans* isomer was so much more stable than the *cis* isomer that there was no equilibrium between the two isomers. In addition, the *trans* isomer showed a chair conformation, whereas the *cis* isomer was in a boat conformation, which indicates that the larger cavity of the six-membered chelating ring of the 5–6–5 rings stabilized the latter conformation. In addition, the optimization of the copper complexes was also carried out by using pseudopotential SDD, but the energy difference of the isomers (*cis*- and *trans*- of $[CuL^1]^{2+}$) was small (0.9 kcal mol^{-1}); this suggests that the LANL2DZ pseudopotential is suitable for these types of complexes.[40]

When two perchlorate ions with the $Cu^{II}L^1$ structure were optimized, it is interesting to note that the *cis*-$[CuL^1]^{2+}$ had a capability of accommodating one perchlorate ion in the axial position, which was stabilized through H-bonding with both NCH_3 groups, which resulted in the formation of a square pyramidal geometry (Figure 8); this is consistent with its X-ray structure (Figure 9): one perchlorate was positioned in the square pyramidal structure, which was proved by the molecular orbital interaction (Figure 10). Furthermore, although the *cis* and *trans* conformations were in equilibrium, the *trans* isomer was unable to

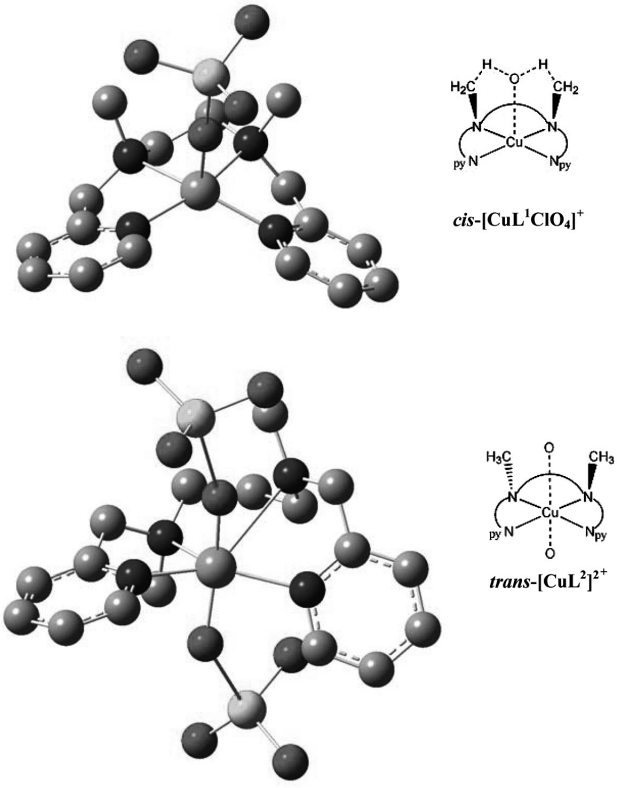

Figure 8. The stable optimized geometries *cis*-$[CuL^1(ClO_4)]^+$ and *trans*-$[CuL^2]^{2+}$.

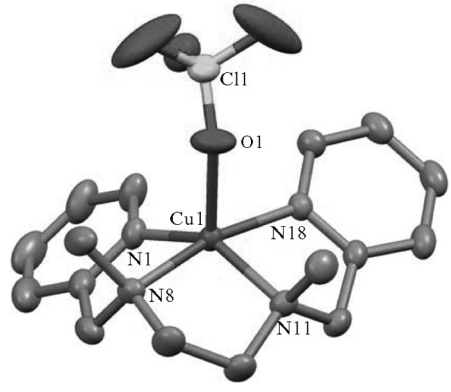

Figure 9. Structure of cation in complex **1** with displacement ellipsoids at the 30% probability level. Hydrogen atoms and disordered O atoms in the perchlorate ligand are omitted for clarity. Selected coordination bond lengths (Å) and angles (°): Cu1–N1 1.996(3), Cu1–N8 2.031(3), Cu1–N11 2.028(3), Cu1–N18 2.000(3), Cu1–O1 2.246(4), Cu1–O1′ 2.241(7); N1–Cu1–N11 145.29(13), N8–Cu1–N18 167.92(12).

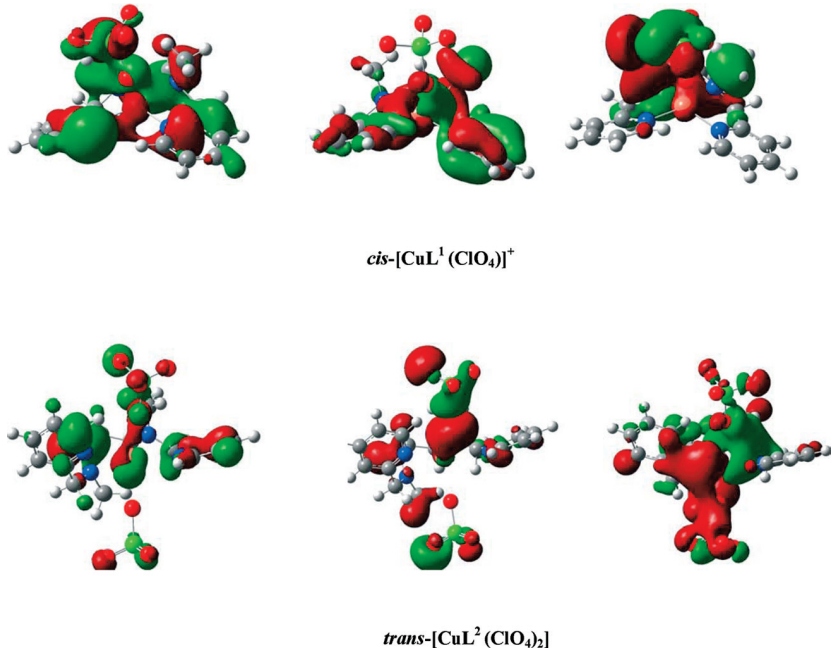

Figure 10. Molecular orbital HOMO–LUMO interaction in *cis*-$[CuL^1(ClO_4)]^+$ and in *trans*-$[CuL^2(ClO_4)_2]$.

retain the perchlorate ion in a coordination sphere, as both NCH_3 groups were in the *trans* position and unable to form a H-bond with the perchlorate ion. In the case of $[CuL^2]^{2+}$, where only one *trans* isomer was possible, there was no H-bond formation between NCH_3 and the perchlorate ion, but a larger chelating ring (5–6–5) around the Cu^{II} center facilitated the accommodation of two perchlorate ions in the axial positions, which resulted in an octahedral geometry (Figures 8 and 10). This is also in agreement with its X-ray structure analysis (Figure 11).

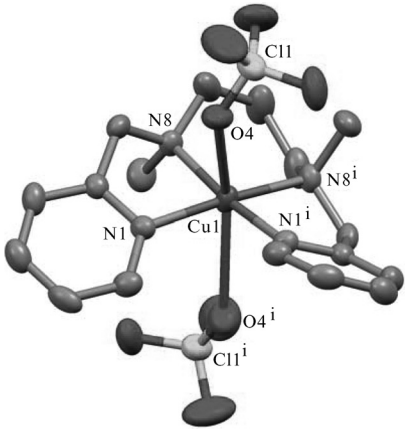

Figure 11. Structure complex **2** with displacement ellipsoids at the 30% probability level. Hydrogen atoms and disordered O atoms in the perchlorate ligands are omitted for clarity. Symmetry code for labeled *i* atoms: $1 - x, y, 1/2 - z$. Selected coordination bond lengths (Å) and angles (°): Cu1–N1 1.990(4), Cu1–N8 2.042(4), Cu1–O4 2.736(7), Cu1–O4′ 2.493(11); N8–Cu1–$N1^i$ 171.63(18), O4–Cu1–$O4^i$ 152.7(3), O4′–Cu1–$O4'^i$ 169(2).

X-ray Crystal Structures

Both complexes are a monomeric species based on a Cu^{II} metal center. In the case of **1** (Figure 9), the metal center is clearly five-coordinate through four N atoms of the ligand and one O atom of a ClO_4^-, whereas another ClO_4^- anion remains uncoordinated (shortest nonbonding Cu···O separation: 3.95 Å). The coordination geometry may be considered as a tetrahedral distorted square-pyramidal environment with the apical position occupied by the O atom. The conformation of the L^1 ligand is deformed by comparison with that found in the closely related Cu^{II} cationic complex including chloride in place of the perchlorate ligand.[41] For instance, the dihedral angle between the pyridine rings is 59.85(12)° in **1** and 29.93° in the Cl-containing cation. Such a difference may be due to the steric requirement of the coordinated perchlorate ligand. This deformation of the chelating ligand is also reflected in Cu–N bond lengths, which are stronger in **1** [range: 1.996(3)–2.031(3)] than in the Cl-containing cation [range: 2.031(3)–2.068(3) Å].

Simply by inserting a methylene group in the ligand, a different coordination geometry is stabilized in the solid state: in **2**, the Cu^{II} metal ion lies on a glide plane and is six coordinated by four N atoms of the main L^2 ligand and two *trans*-arranged ClO_4^- ions (Figure 11). The resulting molecular complex has an octahedral coordination geometry with the main tetragonal distortion from an ideal geometry produced by a strong Jahn–Teller (JT) effect. Apical bond lengths Cu1–O4 2.736(7) Å and Cu1–O4′ 2.493(11) Å are very long (site occupation factors are 0.75 and 0.25 for O4 and O4′, respectively). The mean Cu^{II}–O(perchlorate) bond length computed from 128 hits in the CSD[42] is ca. 2.5 Å, which confirms that perchlorate ions are weakly

bonded in **2**. In contrast, the corresponding distance found in complex **1** is 2.241(7)–2.246(4) Å. This corresponds to a strong coordination. Unfortunately, the origin of this strong JT distortion remains obscure, because **2** represents the first X-ray characterized Cu^{II} complex containing L^2 as a ligand. A few complexes including the same ligand have, however, been reported by using Ni^{II}[43] or Fe^{II}[44] as metal centers. As for **1**, the conformation of the ligand is affected by the nature of the metal and ancillary ligands. Methyl groups substituting amine N atoms may be arranged *trans* with respect to the N_4 equatorial plane, as in complex **2**, but also in a *cis* configuration, as found in some Fe^{II} complexes.[44] The dihedral angle between the pyridine rings also spans a large range in this family of compounds, from 11.0 to 73.0° [54.1(2)° for **2**]. All these features reflect a degree of flexibility for these ligands, although this character is more pronounced for the diaminopropane-based ligand (complex **2**) than for the diaminoethane-based one (complex **1**).

Electronic Spectra

For all the compounds, the spectra were recorded in methanol, and the band positions with molar absorption coefficients for the complexes are presented in Table 2. After analyzing the electronic spectra recorded in methanol, it was found that even in the methanolic solution, a five-coordinate geometry for **1** yielded a broad-band absorption around 600 nm, which suggests the presence of a square-pyramidal structure that generally exhibits a band in the 550–660 nm range (d_{xy}, $d_{yz} \rightarrow d_{x^2-y^2}$); in addition, the average of the energy of the band is characteristic for a five coordinated geometry.[45,46] Furthermore, as the d–d band is broad, the geometrical isomers such as *cis* and *trans* are unresolved in the spectra; however, the spectra of **1** in DMF becomes a broader band than it does in MeOH because of the greater interaction of DMF with the complex. For **2**, the visible spectrum is slightly shifted to lower energy (675 nm), which is indicative of the presence of an elongated octahedral geometry.[47] The electronic spectra of all the complexes display characteristic absorptions at 270–290 nm assigned to the pyridyl $\pi \rightarrow \pi^*$ transitions. The complexes also show absorption of moderate intensity between 312 and 330, which may be due to a LMCT transition. Furthermore, the d–d unresolved spectra of the *cis* and *trans* isomers were interpreted by calculating the spectral bands for the isomers; TD-DFT calculations were performed with GAUSSIAN 03 with UB3PW91 level of theory by using the LANL2DZ for Cu^{2+} and the 6-311++G** basis set for all other atoms to determine the spectroscopic data, and the results show that there are three bands corresponding to electronic transitions, d_{xz}, $d_{yz} \rightarrow d_{x^2-y^2}$, $d_{xy} \rightarrow d_{x^2-y^2}$, and $d_{z^2} \rightarrow d_{x^2-y^2}$ for the complexes, which confirms the existence of considerable spectral differences for the *cis* and *trans* isomers. For example, the TD-DFT calculated spectroscopic data for *cis*-$[CuL^1ClO_4](ClO_4)$ were 541.8, 510.8, and 484.3 nm, whereas for *trans*-$[CuL^1](ClO_4)_2$ they were 502.0, 472.2, and 469.2 nm. Similarly, the three bands (670.6, 578.7, 555.4 nm) for *trans*-$[CuL^2](ClO_4)_2$ and those of the *cis* isomer (513.9, 494.9, 472.1 nm) resulted.

Table 2. Electronic absorption spectroscopic data of copper(II) compounds with λ_{max} (nm) values and ε ($M^{-1}cm^{-1}$) values in parentheses.[a]

Compounds	d–d bands	CT bands
1	590 (420)	315 (715)
2	605 (440)	320 (730)
3	675 (430)	310 (700)
4	680(435)	330 (740)

[a] Concentrations: a ≈ 1.0×10^{-2} M, b ≈ 1.0×10^{-3} M.

Electrochemical Studies

The redox behavior of the ligands (L^1 and L^2) and their Cu^{II} complexes was studied by cyclic voltammetry (CV) on a glassy carbon electrode by using NBu_4PF_6 as a supporting electrolyte. The electrochemical data are presented in Table 3. The cathodic and anodic shifts of the reduction and oxidation wave increased when the scan rates increased because of the heterogeneous electron-transfer kinetics of the non-Nernstian behavior.[48]

Table 3. Electrochemical data[a] of Cu^{II} complexes at 25 °C.

	Solvents	*E*pc	*E*pa
L^1	MeCN	–0.37, –1.38, –2.17	0.87, 1.17, 1.52, 2.13
$[CuL^1]^{2+}$	MeOH	–0.320, –0.608	–0.242
	MeCN	–0.356	0.148
L^2	MeCN	–0.40, –1.35, –2.19	0.91, 1.23, 1.50, 2.13
$[CuL^2]^{2+}$	MeOH	–0.312, –0.607	–0.238
	MeCN	–0.362	0.142

[a] Peaks correspond to ligands signals. Measured vs. nonaqueous silver reference electrode; supporting electrolyte NBu_4PF_6; scan rate 50 $mV s^{-1}$.

Redox Chemistry of L^1 and L^2

The CV of L^1 and L^2 (6.43×10^{-3} g, 0.0024 mM) in acetonitrile was recorded, and the stability of peaks was confirmed by scanning the voltammograms in variable $E_{+\lambda}$ or $E_{-\lambda}$, ($E_{+\lambda}$ for a positive sweep voltammogram and $E_{-\lambda}$ for a negative sweep voltammogram). For L^1, in the positive-going voltammogram (Figure 12), four prominent irreversible peaks (I_A, II_A, III_A, and IV_A) were at 0.434, 0.717, 1.057, and 1.930 V. The voltammogram with variable switching potential $E_{+\lambda}$ suggests that only four prominent products resulted during the process of oxidation. When the voltammogram was reversed, three irreversible cathodic peaks (II_C, III_C, and IV_A) at –1.603, –2.136, and –2.760 V were detected; in the negative sweep voltammogram, four peaks resulted as well. The stability of both anodic and cathodic signals was analyzed by recording the voltammogram with variable $E_{+\lambda}$, which confirms that L^1 produces stable oxi-

dation products. The ligand L^2 also generated voltammograms similar to those of L^1, which signifies that the ligands are structurally very similar in the production of similar types of oxidation products.

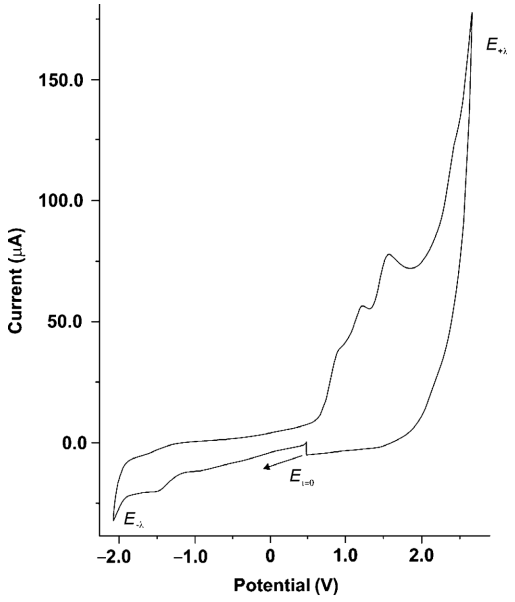

Figure 12. Cyclic voltammogram of L^1 in methanol (2.6×10–3 mmol) at 25 °C. Supporting electrolyte: NBu_4PF_6 (0.1 mol).

Electrochemistry of Copper(II) Complexes

The electrochemical behavior of the copper(II) complexes (2.16×10^{-2} g, 8.11×10^{-2} M) was studied in 0.20 M of Bu_4NPF_6 in DMF and MeOH solutions. For $[CuL^1ClO_4]^+$ in DMF (Figure 13a), an irreversible cyclic voltammogram was obtained for reductions and their corresponding oxidations processes; however, in MeOH, the voltammogram (Figure 13b) became reversible (Ia–Ic) with an additional irreversible reduction peak (IIa) at –0.608 V. Furthermore, in the potential interval 0.5 to –1.5 V, ligand signals did not appear. For the Cu^{II}/Cu^{I} reversible process, the potential peak difference value ($\Delta Ep = Epa - Epc$) was 78 mV, which is characteristic of a monoelectronic quasireversible process. Furthermore, several voltammograms (Figure 14) with different scan rates (v_B) were recorded in the potential interval 0.15 to –0.40 V/Fc^+–Fc to determine the half-wave potential value ($E_{1/2}$ = –0.280 V) for the Cu^{II}–Cu^{I} process (Ia/Ic peaks). The voltammograms (Figure 2) showed a small logarithmic variation of v_B (9.0 mV dec^{-1}), which indicates the presence of a coupled chemical reaction. In addition, in DMF, the partial dissociation of the complex formed two different species, probably $[CuL^1ClO_4]^+$ and $[CuL^1]^{2+}$. This is consistent with the molar conductivity value, which was higher than expected in a 1:1 electrolyte. In methanol, the molar conductivity value for $[CuL^1ClO_4]^+$ was twice that of DMF, which corresponds to a 1:2 electrolyte, probably due to the formation of the $[CuL^1]^{+2}$ species. However, the electrochemical behavior in methanol can be useful to determine the redox properties of the Cu^{II} ion. For $[CuL^2](ClO_4)_2$, a similar redox behavior was obtained in both MeOH and MeCN. This indicates that *cis* and *trans* geometrical isomers of the complexes are unresolved.

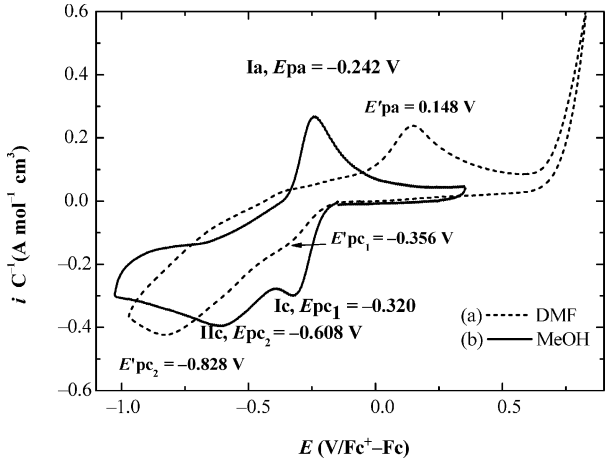

Figure 13. Voltammograms of $[CuL^1ClO_4]ClO_4$, at 100 mV s^{-1} over glassy carbon electrode (C_{glassy}); Bu_4PF_6 (0.1 M) was used as electrolyte: (a) in DMF and (b) in MeOH.

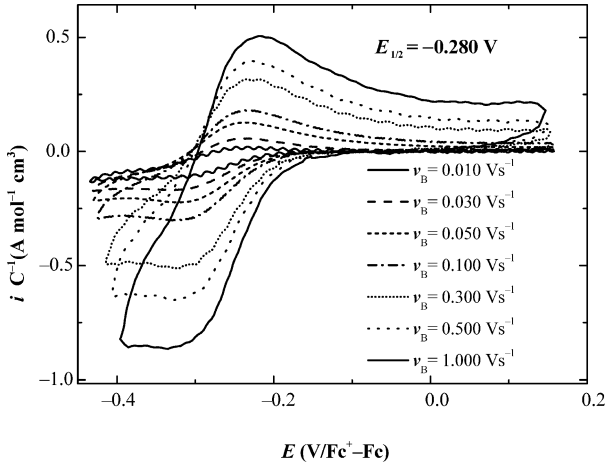

Figure 14. Voltammograms of $[CuL^1ClO_4]ClO_4$ over glassy carbon electrode (C_{glassy}) with different scan rates in MeOH. Bu_4PF_6 (0.1 M) was used as electrolyte.

Conclusions

Spectral and structural studies of ligands show that the conventional and nonconventional H-bonds present in L^1 and L^2 considerably change the chemical environment of the adjacent carbon atoms at protonation sites (pyridyl and tertiary nitrogen atoms) and influence the NMR chemical shifts at different pH values. For the copper complex of L^1, *cis* and *trans* geometrical isomers are in equilibrium with each other, which is in contrast to $[CuL^2]^{2+}$, where the *trans* isomer is unable to equilibrate with the *cis* isomer owing to a greater energy difference (ΔE = 3.9 kcal mol^{-1}) between the two isomers. Indeed, only in *cis*-$[CuL^1]^{2+}$ was the perchlorate ion able to enter its coordination sphere to form

the square pyramidal geometry by stabilizing the structure by H-bonds through two *cis* NCH_3 groups. The *trans* isomer was unable to retain the perchlorate ion in the coordination sphere because the NCH_3 groups were in a *trans* position; this disfavored the presence of the perchlorate ion in the sphere as a result of the absence of H-bonds. This is consistent with the X-ray structure in which *cis*-$[CuL^1(ClO_4)]^+$ is resolved, whereas the *trans* isomer is not.

Experimental Section/Computational Details

Materials: Commercially available reagents were employed without purification: *N*,*N*′-dimethylethylenediamine, *N*,*N*′-dimethyl-1,3-diaminopropane, potassium hydroxide (J. T. Baker), deuterated methanol, deuterated dimethyl sulfoxide, tetramethylsilane, $Cu^{II}(ClO_4)_2{\cdot}6H_2O$, $Cu^{II}Cl_2{\cdot}6H_2O$ (Aldrich). Tetra-*n*-butylammonium bromide and tetrabutylammonium hexaflorophosphate (G. F. Smith) were recrystallized twice from aqueous ethanol.

Physical Measurements: Elemental analyses were carried out with a Fisons (Model EA 1108 CHNSO) and the electronic spectra were measured with a Perkin–Elmer Lambda-900 double beam UV/Vis/NIR spectrophotometer. NMR spectra were recorded by using TMS as an internal standard with Varian Gemini (300 MHz) spectrometers and GC–MS were recorded with a Joel JMS-Axsosha instrument. The pH of the solution was determined with a Conductronic-pH120. Cyclic voltammetry studies were performed at a platinum sphere electrode by using a potentiostat (EG & G PAR 263A) interfaced with a computer having installed EG & G M270 software; the reference electrode was Ag(s)/($AgNO_3$) in methanol; acryocirculator (BRABENDER T-150) was made use of to maintain the temperature (25 ± 0.4 °C) of the electrochemical cell. All the solutions were deoxygenated by bubbling them with research-grade nitrogen. Analytical-grade acetonitrile and methanol purchased from Aldrich were used for electrochemistry.

Computational Procedure: The DFT calculations were performed by means of the Gaussian-03 program[49] for L^1, L^1H^+, L^2, and L^2H^+, as well as for the $[CuL^1]^{2+}$, $[CuL^2]^{2+}$, $[CuL^1(ClO_4)]^+$, and $[CuL^2(ClO_4)_2]$ systems. The exchange correlation was treated at the B3PW91,[50,51] and the choice of this method was based on the results obtained;[52] 6-311++G** was used for C, N, and H atoms, and for Cu^{2+}, LANL2DZ pseudopotential was used.[40] The structures of L^1 and L^2 were fully optimized and their data were then used as the input for the $[CuL^1]^{2+}$ and $[CuL^2]^{2+}$ geometrical optimizations. The charge distribution in the structures was analyzed by Natural Population Analysis. The energies of the frontier molecular orbitals, viz., the highest occupied molecular orbital (HOMO) and HOMO-1 to HOMO-3 and also the lowest unoccupied molecular orbital (LUMO) were derived. Furthermore, the electronic charge density that alters the NMR chemical shifts of the carbon atoms of L^1, L^2, and their protonated species. All computed geometries were verified by frequency calculations to have no imaginary frequencies. NMR chemical shifts were calculated by the GIAO method at the B3PW91/6-311++G(d,p) level, and the chemical shifts were referenced to TMS (GIAO magnetic shielding tensor) 192.6 ppm for carbon atoms and 31.65 ppm for protons in TMS.[53,54] The ground-state wavefunction, which was further applied for "atoms in molecules" (AIM) calculations,[55] was employed to find bond critical points (BCPs) and ring critical points (RCPs). AIM calculations based on the Bader theory were carried out by means of the AIM2000 program.[56] BCPs and RCPs were analyzed in terms of electron densities, ρ, and their Laplacians, $\nabla^2\rho$.

Preparations of Ligands

***N*,*N*′-Dimethyl-*N*,*N*′-bis(pyridin-2-ylmethyl)-1,2-diaminoethane (L^1):** The ligand was synthesized by a modified technique of the reported procedure.[57–60] To a solution of *N*,*N*′-dimethylethylenediamine (6.5 mM) and KOH (25 mM) in nitrogen-flushed methanol (25 mL) was slowly added 2-chloromethylpyridine·hydrochloride (13.0 mM) dissolved in methanol (25 mL) under nitrogen atmosphere. The mixture was stirred for 30 min, heated at reflux for 1 h, and then cooled to room temperature. After the methanol was evaporated from the reaction mixture under vacuum, water was added, followed by KOH to raise the pH to 13. The product was extracted with dichloromethane, and the organic layer was then dried with magnesium sulfate. Subsequently, the solvent was evaporated, and a yellow crystalline solid (1.42 g, 81%) was obtained. ^{1}H NMR (300 MHz, CD_3OD): δ = 2.32 (s, 6 H, -*N*-CH_3), 2.73 (s, 4 H, -CH_2- CH_2-), 3.77 (s, 4 H, -*N*-CH_2-Py), 7.35–7.95 (m, 8 H, pyridine ring) ppm. MS (I): *m*/*z* (%) = 270 $[M]^+$, 271 $[M + 1]^+$, 135 (100) $[C_8H_{11}N_2]^+$, 92 $[C_5H_6N]^+$, 106 $[C_6H_6N_2]^+$, 148 $[C_9H_{11}N_2]^+$. $C_{16}H_{22}N_4$ (270.36): calcd. C 71.08, H 8.20, N 20.72; found C 69.65, H 7.80, N 19.61.

***N*,*N*′-Dimethyl-*N*,*N*′-bis(pyridin-2-ylmethyl)-1,3-diaminopropane (L^2):** The above-mentioned procedure was adopted for the preparation of L^2 by using *N*,*N*′-dimethyl-1,3-diaminopropane (1.44 g, 78%). ^{1}H NMR (300 MHz, CD_3OD): δ = 2.75–3.25 (m, 6 H, -NCH_2-CH_2-CH_2N-), 3.17 (s, 6 H, -CH_3), 4.32 (s, 4 H, Py-CH_2-*N*-), 7.85–725 (m, 8 H, pyridine ring) ppm. MS: *m*/*z* (%) = 284 $[M]^+$, 135 (100) $[C_8H_{11}N_2]^+$, 92 $[C_5H_6N]^+$, 121 $[C_7H_9N]^+$, 149 $[C_9H_{13}N_2]^+$. $C_{17}H_{24}N_4$ (284.38): calcd. C 71.79, H 8.51, N 19.70; found C 71.42, H 8.43, N 19.55.

NMR Spectroscopic Studies at Variable pH: The ligand behavior at different pH values was studied by ^{13}C NMR spectroscopy, and the chemical shift values relative to tetramethylsilane of each carbon atom of the ligands were plotted against pH. NaOD (30% w/w in D_2O) or DCl (37% in D_2O) was used to adjust the pH of the ligand solution, and its concentration was approximately 0.01 mol dm^{-3}.

Copper(II) Complexes

$[CuL^1(ClO_4)](ClO_4)$ (1): To a solution of L^1 (1.0 mmol) dissolved in methanol (10.0 mL) was added a solution of $Cu(ClO_4)_2{\cdot}6H_2O$ (1.0 mmol) in methanol (5.0 mL). The resulting solution was kept at room temperature for slow evaporation to produce blue crystals (0.49 g, 93%) and suitable single crystals were obtained for X-ray diffraction. $[CuC_{16}H_{22}N_4ClO_4]ClO_4$ (531.99): calcd. C 36.12, H 4.17, N 10.53; found C 35.96, H 4.25, N 10.39.

$[CuL^2](ClO_4)_2$ (2): To a solution of L^2 (1.0 mmol) dissolved in methanol (10.0 mL) was added a solution of $Cu(ClO_4)_2{\cdot}6H_2O$ (1.0 mmol) in methanol (5.0 mL). The resulting solution was kept at room temperature for slow evaporation to generate purple crystals (49 g, 89%) and suitable single crystals were obtained for X-ray diffraction. $CuC_{17}H_{24}N_4(ClO_4)_2$ (546.01): calcd. C 37.39, H 4.43, N 10.26; found C 37.56, H 4.35, N10.39.

The above procedure was applied to prepare the following copper compounds by using ligands L^1 and L^2 with the respective copper(II) salts: $[CuL^1]Cl_2{\cdot}2H_2O$ (**3**) (0.40 g, 90%). $CuC_{16}H_{26}N_4Cl_2O_2$ (440.03): calcd. C 43.67, H 5.96, N 12.73; found C 43.45, H 5.83, N 12. 68. $[CuL^2]Cl_2{\cdot}H_2O$ (**4**) (0.37 g, 86%). $CuC_{17}H_{26}N_4Cl_2O$ (436.04): calcd. C 46.82, H 6.01, N 12.85; found C 46.97, H 5.88, N 12.79.

IR Spectra: The presence of uncoordinated ClO_4^- ions in complexes **1** and **2** is supported by the IR spectra, which show an unsplit

Table 4. Crystallographic data for Complexes **1** and **2**.

	1	**2**
Empirical formula	$[Cu(C_{16}H_{22}N_4)(ClO_4)]\ ClO_4$	$Cu(C_{17}H_{24}N_4)(ClO_4)_2$
*F*ormula weight	532.82	546.84
Temperature (K)	300(1)	300(2)
Wavelength (Å)	0.71073	0.71073
Crystal system	triclinic	orthorhombic
Space group	$P\bar{1}$	*Pbcn*
a (Å)	9.0053(8)	9.3731(9)
b (Å)	9.3855(6)	13.7458(9)
c (Å)	12.8078(8)	17.1069(15)
α (°)	85.745(5)	90
β (°)	84.771(6)	90
γ (°)	83.185(6)	90
V (Å^3)	1068.18(13)	2204.1(3)
Z, *Z*′	2, 1	4, 1/2
μ (mm^{-1})	1.324	1.286
$D_{calcd.}$ (Mg m^{-3})	1.657	1.648
Crystal size (mm)	$0.40 \times 0.36 \times 0.18$	$0.28 \times 0.22 \times 0.22$
2θ range (°)	3.2–55.0	4.7–52.0
Measured reflect.	6947	3513
Unique reflect., R_{int}[a]	4912, 0.022	2171, 0.032
Refined parameters	356	183
R indices [$I > 2\sigma(I)$][a]	$R_1 = 0.047$, $wR_2 = 0.115$	$R_1 = 0.062$, $wR_2 = 0.152$
R indices [all data][a]	$R_1 = 0.066$, $wR_2 = 0.125$	$R_1 = 0.099$ $wR_2 = 0.175$
$\Delta\rho_{max}/\Delta\rho_{max}$ (e Å^{-3})	0.51, –0.53	0.88, –0.46

[a] $R_{int} = \Sigma|F_o^2 - <F_o^2>|/\Sigma F_o^2$, $R_1 = \Sigma||F_o| - |F_c||/\Sigma|F_o|$, $wR_2 = [\Sigma w(F_o^2 - F_c^2)^2/\Sigma w(F_o^2)^2]^{1/2}$.

band centered at 1155 cm^{-1}. Although perchlorates are potentially explosive, no accident occurred with the perchlorate complexes during the experimental work.

X-ray Crystallography: X-ray diffraction data for complexes $[CuL^1(ClO_4)](ClO_4)$ (**1**) and $[CuL^2(ClO_4)_2]$ (**2**) were measured on single crystals at 300(1) K by using a Bruker P4 diffractometer equipped with a non-CCD detector.[61] Data were corrected for absorption effects on the basis of *ψ*-scans (**1**) or crystal-face indexation (**2**). A summary for data collection and structure refinements is given in Table 4. In both structures, ClO_4^- anions, disordered by rotation (a common feature for this small anion with a spherical shape), were modeled as distributed over two sites, and site occupation factors were refined and eventually fixed in the last least-squares cycles. The geometry for the ClO_4^- ions was systematically regularized through restraints for distances: Cl–O 1.40(1) Å and O–O = 2.29(1) Å. All H atoms were placed in idealized positions and constrained to ride on their parent atoms. The structures were solved and refined with SHLEXS97 and SHLEXL97 software.[62] CCDC-642108 (for **1**) and -642109 (for **2**) contain the supplementary crystallographic data for this paper. These data can be obtained free of charge from The Cambridge Crystallographic Data Centre via www.ccdc.cam.ac.uk/data_request/cif.

Acknowledgments

The authors acknowledge the Direccíon General de Asuntos del Personal Académico (Project PAPIIT No. IN202706-3) for economic support. We also thank DGSCA-UNAM for computation facilities. J. C. deeply acknowledges a grant from CONACyT-México.

[1] A. Messerschmit, R. Huber, T. Poulas, K. Wieghardt (Eds.), *Handbook of Metalloproteins*, John Wiley & Sons, Chichester, U. K., **2001**.
[2] I. Bertini, A. Sigel, H. Sigel (Eds.), *Handbook on Metalloproteins*, Marcel Dekker, New York, **2001**.
[3] E. I. Solomon, P. Chen, M. Metz, S.-K. Lee, A. E. Palmer, *Angew. Chem. Int. Ed.* **2001**, *40*, 4570–4590.
[4] E. I. Solomon, R. K. Szilagyi, S. D. Geroge, L. Basumallick, *Chem. Rev.* **2004**, *104*, 419–458.
[5] D. B. Rorabacher, *Chem. Rev.* **2004**, *104*, 651–698.
[6] G. Henkel, B. Kreb, *Chem. Rev.* **2004**, *104*, 801–824.
[7] L. M. Mirica, X. Ottenwaelder, T. D. P. Stack, *Chem. Rev.* **2004**, *104*, 1013–1045.
[8] E. A. Lewis, W. B. Tolman, *Chem. Rev.* **2004**, *104*, 1047–1076.
[9] E. Kim, E. E. Chufan, K. Kamaraj, K. D. Karlin, *Chem. Rev.* **2004**, *104*, 1077–1133.
[10] E. Nakamura, S. Mori, *Angew. Chem. Int. Ed.* **2000**, *39*, 3750–3771.
[11] A. W. Thomas, S. V. Ley, *Angew. Chem. Int. Ed.* **2003**, *42*, 5400–5449.
[12] I. P. Beletskaya, A. V. Cheprakov, *Coord. Chem. Rev.* **2004**, *248*, 2337–2364.
[13] T. Pintauer, K. Matyjaszewski, *Coord. Chem. Rev.* **2005**, *249*, 1155–1184.
[14] R. Machida, E. Kimura, M. Kodama, *Inorg. Chem.* **1983**, *22*, 2055–2061.
[15] M. Meyer, L. Frémond, E. Espinosa, R. Guilard, Z. Ou, K. M. Kadish, *Inorg. Chem.* **2004**, *43*, 5572–5587.
[16] J. P. Klinman, *Chem. Rev.* **1996**, *96*, 2541–2562.
[17] E. I. Solomon, U. M. Sundaram, T. E. Machonkin, *Chem. Rev.* **1996**, *96*, 2563–2606.
[18] S. Schindler, *Eur. J. Inorg. Chem.* **2000**, 2311–2326.
[19] A. P. Cole, D. E. Root, P. Mukherjee, E. I. Solomon, T. D. P. Stack, *Science* **1996**, *273*, 1848–1850.
[20] K. D. Karlin, *Science* **1993**, *261*, 701–708.
[21] K. D. Karlin, Z. Tyeklar (Eds.), *Bioinorganic Chemistry of Copper*, Chapman & Hall, New York, **1993**.
[22] a) J. G. Gilbert, A. W. Addison, A. Y. Nazarenko, R. Butcher, *J. Inorg. Chim. Acta* **2001**, *324*, 123–130; b) J. G. Gilbert, A. W. Addisonm, P. Prabakaran, R. J. Butcher, G. Bocelli, *Inorg. Chem. Commun.* **2004**, *7*, 701–704.

[23] M. S. Díaz-Cruz, J. Mendieta, A. Monjonell, R. Tauler, M. Esteban, *J. Inorg. Biochem.* **1998**, *70*, 91–98.
[24] K. D. Karlin, A. D. Zuberbühler in *Bioinorganic Catalysis* (Eds.: J. Reedijk, E. Bouwman), M. Decker, New York, **1999**.
[25] A. G. Blackman, W. B. Tolman in *Structure & Bonding* (Ed.: B. Meunier.), Springer, Berlin, Germany, **2000**.
[26] S. A. Leaver, M. Palaniandavar, C. A. Kilner, M. A. Halcrow, *Dalton Trans.* **2003**, 4224–4225.
[27] M. Costas, M. P. Mehn, M. P. Jensen, L. Que, *Chem. Rev.* **2004**, *104*, 939–986.
[28] J. Zhang, H. Zheng, S. L. Groce, J. D. Lipscomb, *J. Mol. Catal. A* **2006**, *251*, 54–65.
[29] S. Groni, G. Blain, R. Guillot, C. Policar, E. Anxolabéhére-Mallart, *Inorg. Chem.* **2007**, *46*, 1951–1953.
[30] M. Martinho, F. Banse, J. Sainton, C. Philouze, R. Guillot, G. Blain, P. Dorlet, S. Lecomte, J. J. Girerd, *Inorg. Chem.* **2007**, *46*, 1709–1717.
[31] G. A. Jeffrey, W. Saenger, *Hydrogen Bonding in Biological Structures*, Springer, Berlin, **2006**.
[32] G. R. Desiraju, T. Steiner, *The Weak Hydrogen Bond in Structural Chemistry and Biology*, Oxford University Press Inc., New York, **1999**.
[33] S. Scheiner, S. J. Grabowski, *J. Mol. Struct.* **2002**, *615*, 209–218.
[34] M. Domagala, S. J. Grabowski, K. Urbaniak, G. Mloston, *J. Phys. Chem. A* **2003**, *107*, 2730–2736.
[35] G. R. Desiraju, *Angew. Chem. Int. Ed. Engl.* **1995**, *34*, 2311–2321.
[36] M. Domagala, S. J. Grabowski, *J. Phys. Chem. A* **2005**, *109*, 5683–5688.
[37] M. Domagala, S. J. Grabowski, K. Urbaniak, G. Mloston, *J. Mol. Struct.* **2004**, *690*, 69–75.
[38] R. G. Pearson, *J. Chem. Educ.* **1999**, *76*, 267–275.
[39] R. G. Pearson, *Inorg. Chim. Acta* **1998**, *270*, 252–260.
[40] P. J. Hay, W. R. Wadt, *J. Chem. Phys.* **1985**, *82*, 299–310.
[41] Y. Kani, S. Ohba, M. Kunita, Y. Nishida, *Acta Crystallogr., Sect. C* **2000**, *56*, e197–199.
[42] F. H. Allen, *Acta Crystallogr., Sect. B* **2002**, *58*, 380–388.
[43] H. J. G. Hernández, T. Pandiyan, S. Bernes, *Inorg. Chim. Acta* **2006**, *359*, 1–12.
[44] R. Mas-Ballesté, M. Costas, T. van den Berg, L. Que Jr, *Chem. Eur. J.* **2006**, *12*, 7489–7500.
[45] S. J. Brudenell, L. Spiccia, E. R. T. Tiekink, *Inorg. Chem.* **1996**, *35*, 1974–1979.
[46] G. A. McLachlan, G. D. Fallon, R. E. Martin, L. Spiccia, *Inorg. Chem.* **1995**, *34*, 254–261.
[47] a) A. C. van Steenberg, E. Bouwman, G. de Graaff, W. L. Driessen, J. Reedijk, P. Zanello, *J. Chem. Soc., Dalton Trans.* **1990**, 3175; b) M. Palaniandavar, T. Pandiyan, M. Lakshminarayanan, H. Manohar, *J. Chem. Soc., Dalton Trans.* **1996**, 455–461.
[48] A. J. Bard, L. R. Faulkner, *Electrochemical Methods: Fundamental Applications*, Wiley, New York. **1990**. pp. 213–241.
[49] M. J. Frisch, G. W. Trucks, H. B. Schlegel, G. E. Scuseria, M. A. Robb, J. R. Cheeseman, J. A. Montgomery Jr, T. Vreven, K. N. Kudin, J. C. Burant, J. M. Millam, S. S. Iyengar, J. Tomasi, V. Barone, B. Mennucci, M. Cossi, G. Scalmani, N. Rega, G. A. Petersson, H. Nakatsuji, M. Hada, M. Ehara, K. Toyota, R. Fukuda, J. Hasegawa, M. Ishida, T. Nakajima, Y. Honda, O. Kitao, H. Nakai, M. Klene, X. Li, J. E. Knox, H. P. Hratchian, J. B. Cross, C. Adamo, J. Jaramillo, R. Gomperts, R. E. Stratmann, O. Yazyev, A. J. Austin, R. Cammi, C.Pomelli, J. W. Ochterski, P. Y. Ayala, K. Morokuma, G. A.Voth, P. Salvador, J. J. Dannenberg, V. G. Zakrzewski, S. Dapprich, A. D. Daniels, M. C. Strain, O. Farkas, D. K. Malick, A. D. Rabuck, K. Raghavachari, J. B. Foresman, J. V. Ortiz, Q. Cui, A. G. Baboul, S. Clifford, J. Cioslowski, B. B. Stefanov, G. Liu, A. Liashenko, P. Piskorz, I. Komaromi, R. L. Martin, D. J. Fox, T. Keith, M. A. Al-Laham, C. Y. Peng, A. Nanayakkara, M. Challacombe, P. M. W. Gill, B. Johnson, W. Chen, M. W. Wong, C. Gonzalez, J. A. Pople, *Gaussian 03*, revision D.01, Gaussian, Inc., Wallingford, CT, **2004**.
[50] A. D. Becke, *J. Chem. Phys.* **1993**, *98*, 5648–5652.
[51] a) J. P. Perdew in *Electronic Structure of Solids* (Eds.: P. Ziesche, H. Eischrig), Akademie Verlag, Berlin, **1991**; b) J. P. Perdew, Y. Wang, *Phys. Rev. B* **1992**, *45*, 13244–13249; c) A. D. Becke, *J. Chem. Phys.* **1993**, *98*, 5648–5652; d) J. P. Perdew, K. Burke, Y. Wang, *Phys. Rev. B* **1996**, *54*, 16533.
[52] P. M. Waller, H. Braun, N. Hjdis, M. Buhl, *J. Chem. Theory Comput.* **2007**, *3*, 2234–2242.
[53] K. Wolinski, J. F. Hinton, P. Pulay, *J. Am. Chem. Soc.* **1990**, *112*, 8251–8260.
[54] R. Ditchfield, *Mol. Phys.* **1974**, *27*, 789–807.
[55] R. F. W. Bader, *Atoms in Molecules: A Quantum Theory*, Oxford University Press, New York, **1990**.
[56] F. Biegler-Konig, *AIM2000*, University of Applied Sciences, Bielefeld, Germany.
[57] T. Pandiyan, S. Bernès, C. Durán de Bazúa, *Polyhedron* **1997**, *16*, 2819–2826.
[58] T. Pandiyan, R. Enríquez, M. A. Bernés, S. C. Durán de Bazúa, *Polyhedron* **1999**, *18*, 3383–3390.
[59] T. Pandiyan, V. M. Consuelo-Estrada, R. Moreno-Esparza, L. Ruiz-Ramírez, *Inorg. Chim. Acta* **2003**, *343*, 79–89.
[60] R. P. F. Kanter, R. Yu, A. W. Addison, *Inorg. Chim. Acta* **1992**, *196*, 97 –103.
[61] *XSCAnS Users Manual*, release 2.21, Siemens Analytical X-ray Instruments Inc., Madison, WI, **1996**.
[62] G. M. Sheldrick, *SHELX97 Users Manual*, University of Göttingen, Germany, **1997**.

Received: January 25, 2008
Published Online: June 24, 2008

